Progress In Electromagnetics Research C, Vol. 130, 57–67, 2023

Active Disturbance Rejection Sensorless Control of Permanent Magnet Synchronous Motor Based on the Fuzzy Neural Network Left Inverse System

Xin Liu[1], Yanfei Pan[2], Lin Wang[2], Jiping Li[3], Yilin Zhu[2, *], Jian Xu[2] and Xiuwen Luo[2]

Abstract—A sensorless control method based on active disturbance rejection control (ADRC) and left inverse of a fuzzy neural network is proposed to realize the sensorless control of permanent magnet synchronous motor (PMSM) for machine tools. Firstly, on the basis of analyzing the mathematical model of PMSM and the theory of left inverse system, a left inverse system observer is constructed. Secondly, after verifying the left reversibility of the PMSM control system, the fuzzy neural network is used to construct the left inverse system, and the left inverse system is connected with the PMSM control system in series to realize the sensorless control of the PMSM. Thirdly, according to the mathematical model of PMSM and the sensorless speed observation results, an ADRC method to improve the sensorless control effect is proposed. Finally, the experimental platform of the sensorless control method based on ADRC fuzzy neural network left inverse is built. The experimental results show that the method can estimate the speed and position well.

1. INTRODUCTION

The permanent magnet synchronous motor (PMSM) is widely used in machine tools because of its simple structure, wide speed range, small size, high power density, and high efficiency. The encoder can detect the speed and position signals of PMSM in real time. However, the actual environment and operating conditions are complex and harsh during the machining process of the machine tool [1, 2]. Therefore, if the encoder fails, the machining process will be seriously affected. In recent years, sensorless control has grown quickly. High-performance sensorless control is lacking, though. The sensorless control algorithm of the high-speed PMSM control system needs to be studied.

At present, the back extended electromotive force (EMF) [3–5], high-frequency injection method [6, 7], extended Kalman filter [8,9], and model reference adaptive system [10,11] are the primary approaches used for common sensorless control of permanent magnet synchronous motors. Sensorless control based on the back EMF model has the advantages of simple structure, low computation, good dynamic response, etc., but requires accurate motor parameters. In the actual operation process of the motor, the motor parameters are easy to change, resulting in poor sensorless control performance. Especially in zero speed and low speed operation, the back EMF of the motor is small, and it is difficult to obtain effective position and speed information from the back EMF at this time [12]. According to the back EMF model, many different observers can be constructed to observe the rotor position and speed. Among them, sliding mode observer is a common method, which is robust and easy to implement. However, this method is a special nonlinear control system with discontinuity. Once sliding mode state is entered, the observer will chatter, which will reduce the overall stability of the system [3–5].

Received 24 November 2022, Accepted 8 February 2023, Scheduled 20 February 2023
* Corresponding author: Yilin Zhu (yl.zhu.dy@gmail.com).
[1] Beijing Machinery Industry Automation Research Institute Co., Ltd., Beijing 100120, China. [2] Jiangsu Changjiang Intelligent Manufacturing Research Institute Co, Ltd., Changzhou 213001, China. [3] Qinhuangdao Customs Coal Testing Technology Center, Qinhuangdao 066000, China.

Because of the salient pole characteristic of permanent magnet motor, the rotor position can be obtained by applying additional high-frequency signals. The method needs to inject additional high-frequency signal, which has a certain adverse effect on the motor performance. At the same time, this method has a strong dependence on the salient pole characteristics of the rotor [6, 7]. Extended Kalman filter can effectively suppress various noises and accurately obtain rotor position and speed by configuring corresponding covariance matrix. However, this method is greatly affected by external factors, and the change of motor parameters will also greatly affect the observation performance [8, 9]. The model reference adaptive method can gradually converge the estimated parameters to a stable state. At the same time, the method is simple in operation and has strong anti-interference ability, but it is sensitive to changes in motor parameters, so the parameter robustness is poor [10, 11].

Compared with the traditional sensorless control, the left inverse soft measurement method has strict mathematical theoretical derivation. It clearly gives the mathematical relationship and physical significance between the estimated quantity and the known quantity. This method has opened up a field for indirect measurement [13]. Based on the left inverse system theory, the left inverse model of PMSM is established, and the fuzzy neural network algorithm is used to solve the problem that the left inverse model is difficult to obtain. At the same time, the ADRC is used as the regulator of the speed loop, so that the performance of the sensorless algorithm control is significantly improved.

This paper is mainly divided into five sections, and the specific arrangements are as follows. In Section 2, the mathematical model of PMSM and the algorithm structure of ADRC are constructed. In Section 3, the basic left inverse system and the sensorless control algorithm based on fuzzy neural network left inverse system structure are given. In Section 4, the proposed algorithm is tested and analyzed. Finally, the full text is summarized in Section 5.

2. MATHEMATICAL MODEL AND ADRC SYSTEM OF PERMANENT MAGNET SYNCHRONOUS MOTOR

2.1. Mathematical Model of the PMSM

The mathematical model [1, 2] of PMSM in d- and q-axis coordinate system is

$$\begin{cases} pi_d = -\dfrac{R_s}{L_d} i_d + \dfrac{L_q}{L_d}\omega_e i_q + \dfrac{u_d}{L_d} \\ pi_q = -\dfrac{R_s}{L_q} i_q - \dfrac{L_d}{L_q}\omega_e i_d - \dfrac{1}{L_q}\omega_e \lambda_f + \dfrac{u_q}{L_q} \end{cases} \tag{1}$$

where p is the differential operator; u_d, u_q, i_d, and i_q are voltages and currents in d- and q-axis, respectively; R_s is the stator resistance; λ_f is the flux linkage of permanent magnet; L_d and L_q are inductances in d- and q-axis, respectively; ω_e is the electrical angular velocity.

The expression of electromagnetic torque and mechanical motion equation [2] is

$$\begin{cases} T_e = 1.5 n_p [\lambda_f i_q + (L_d - L_q) i_d i_q] \\ \dfrac{d\omega_e}{dt} = \dfrac{n_p (T_e - T_L - B\omega_m)}{J} \end{cases} \tag{2}$$

where ω_m is the mechanical angular velocity of motor, T_e the electromagnetic torque, T_L the load torque, B the viscous damping, J the moment of inertia, and n_p the number of pole pairs.

2.2. Establishment of PMSM Active Disturbance Rejection Control System

The ADRC can simplify the controlled object and extended state observer (ESO) into an integral series system by reasonably configuring the parameters of the ESO. At this time, the state error feedback (SEF) is designed to make the system have a good control effect.

According to (2), the electromagnetic torque is substituted into the motor speed expression, and the mechanical motion expression can be rewritten as

$$\frac{d\omega_e}{dt} = \frac{1}{J}\left[1.5 n_p^2 \left(\lambda_f i_q + (L_d - L_q)\, i_d i_q\right) - n_p T_L - B\omega_e\right] \tag{3}$$

It can be seen from (3) that the motor speed is affected by i_d, i_q, and T_L. According to the ADRC principle, $\frac{1}{J}\left[1.5n_p^2\left(L_d - L_q\right)i_d i_q - n_p T_L - B\omega_e\right]$ in (3) is regarded as the disturbance f_w; i_q is selected as the input signal u, $\frac{1.5n_p^2\lambda_f}{J}$ as the coefficient b. The mechanical motion expression can be rewritten as

$$\frac{d\omega_e}{dt} = \frac{1}{J}1.5n_p^2\lambda_f i_q + f_w = bu + f_w \tag{4}$$

The structure of the designed PMSM sensorless ADRC system is shown in Figure 1. It can be seen from Figure 1 that the ADRC of speed loop consists of two links, namely linear extended electromotive force (LESO) and linear state error feedback (LSEF). ADRC uses LESO to estimate the controlled object. In this process, it can not only obtain the estimated values of various state variables, but also estimate the total disturbance of the system and use the estimated total disturbance to compensate the LSEF control system [2].

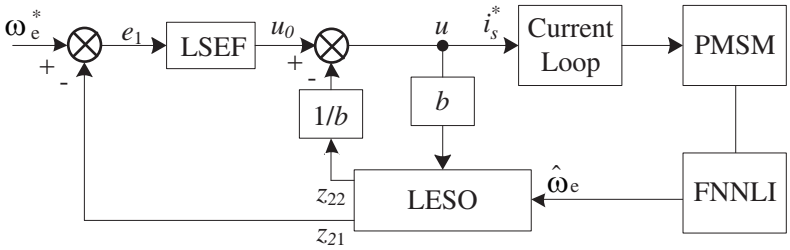

Figure 1. Sensorless ADRC control system for PMSM.

The calculation process [2] inside LESO can be expressed as

$$\begin{cases} e_0 = z_{21} - \hat{\omega}_e \\ \dot{z}_{21} = z_{22} - \beta_1 e_0 + bu \\ \dot{z}_{22} = -\beta_2 e_0 \end{cases} \tag{5}$$

where z_{21} is the speed signal observed by LESO; $\hat{\omega}_e$ is the motor speed observed by fuzzy neural network left inverse (FNNLI) algorithm; z_{22} is the total disturbance observed by LESO; β_1 and β_2 are the observer coefficients of LESO.

The calculation process [2] inside LSEF can be expressed as

$$\begin{cases} e_1 = \omega_e^* - z_{21} \\ u_0 = \beta_3 e_1 \end{cases} \tag{6}$$

where β_3 is the coefficient of LSEF, and u_0 is the output of LSEF controller.

The compensation output [2] of the disturbance is

$$u = u_0 - \frac{z_{22}}{b} \tag{7}$$

FNNLI algorithm sends the observed motor speed to ADRC control algorithm for closed-loop speed control, and the total disturbance of the system is observed through LESO to achieve high-performance control effect. FNNLI will be analyzed in detail in the following sections.

3. SPEED SENSORLESS CONTROL METHOD OF THE PMSM BASED ON THE FUZZY NEURAL NETWORK LEFT INVERSE

3.1. Left Inverse System Theory of the PMSM

Both the left inverse system and right inverse system belong to different applications in inverse system theory. This strategy is comparable to observability in control theory since the right inverse system can implement system compensation while the left inverse system focuses more on reproducing system input signals. In view of this, the left inverse system theory can realize the estimation of PMSM speed.

The principle of the left inverse system is given as below. For a nonlinear system as follows

$$\dot{\boldsymbol{x}} = f(\boldsymbol{x}, \boldsymbol{u}) \tag{8}$$

where $\boldsymbol{x} = [x_1, x_2, \ldots, x_n]^T$ is the n-dimensional state variable.

If the nonlinear system contains an internal sensor subsystem, the unobservable variable of the original system serves as the internal sensor subsystem's input, while the observable variable of the original system serves as its output. After that, the internal sensor subsystem may be expressed as

$$\boldsymbol{x}_l = f(\boldsymbol{x}_m, \dot{\boldsymbol{x}}_l, \ddot{\boldsymbol{x}}_l, \ldots, \boldsymbol{u}) \tag{9}$$

where $\boldsymbol{x}_m = [x_1, x_2, \ldots, x_m]^T$ is the m-dimensional state variable, and $\boldsymbol{x}_l = [x_{m+1}, x_{m+2}, \ldots, x_{m+n}]^T$ is the $(n-m)$-dimensional state observable variable.

For such a subsystem, if the left inverse system of the system exists, the expression of the left inverse system can be written as follows

$$\boldsymbol{x}_m = f(\boldsymbol{x}_l, \dot{\boldsymbol{x}}_l, \ddot{\boldsymbol{x}}_l, \ldots, \boldsymbol{u}, \dot{\boldsymbol{u}}, \ddot{\boldsymbol{u}}, \ldots) \tag{10}$$

The left inverse system can be characterized in general as follows. Assume that the mapping relationship $u \to y$ is present in the nonlinear system. There is a system like this one whose mapping relationship is $v \to w$. If $v(t) = y(t)$, then $w(t) = u(t)$. Then this system is called the left inverse system of the original system, that is, the original system is left reversible.

The observation schematic diagram of the left inverse system is shown in Figure 2. The structure connects the left inverse system of the internal sensor subsystem to the right side of the nonlinear system on the basis of proving that the subsystem is left reversible. The left inverse system structure can observe the unobservable variables in the nonlinear system. However, because the analytic left inverse system of the speed subsystem is difficult to obtain, the fuzzy neural network and differentiator are used to construct the left inverse system of the PMSM speed subsystem.

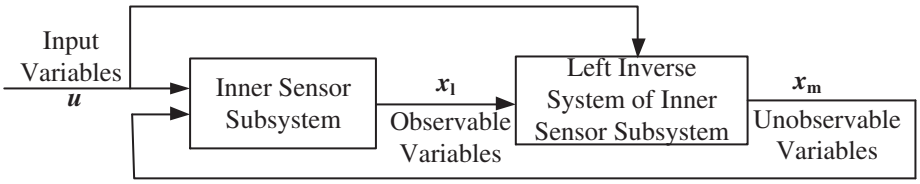

Figure 2. Observation principle of the left inverse system.

3.2. Analysis of the Fuzzy Neural Network Left Inverse System

Equation (1) and Equation (2) can be represented by the following state variables.

$$\begin{cases} \dot{x}_1 = -\dfrac{R_s}{L_d}x_1 + \dfrac{L_q}{L_d}n_p x_2 x_3 + \dfrac{u_1}{L_d} \\ \dot{x}_2 = -\dfrac{R_s}{L_q}x_2 - \dfrac{L_d}{L_q}n_p x_1 x_3 - \dfrac{1}{L_q}n_p \lambda_f x_3 + \dfrac{u_2}{L_q} \\ \dot{x}_3 = -\dfrac{Bx_3}{J} + \dfrac{T_e - T_m}{J} \end{cases} \tag{11}$$

where the observable variables are $x_m = (x_1, x_2)^T = (i_d, i_q)^T$, and the unobservable variables are $x_{um} = x_3 = \omega_e$.

According to (2) to (5), the following equation can be obtained

$$\dot{\boldsymbol{x}} = f(\boldsymbol{x}, \boldsymbol{u}) = \begin{bmatrix} -\dfrac{R_s}{L_d}x_1 + \dfrac{L_q}{L_d}n_p x_2 x_3 + \dfrac{u_1}{L_d} \\ -\dfrac{R_s}{L_q}x_2 - \dfrac{L_d}{L_q}n_p x_1 x_3 - \dfrac{1}{L_q}n_p \lambda_f x_3 + \dfrac{u_2}{L_q} \\ -\dfrac{Bx_3}{J} + \dfrac{T_e - T_m}{J} \end{bmatrix} \tag{12}$$

The correlation can be determined by calculating the partial derivative of the unobservable variable x_3 and the rank of the corresponding matrix. The matrix composed of these ranks is called the Jacobian matrix, which can be written as

$$\mathbf{A} = \left[\frac{\partial x_1}{\partial x_3} \quad \frac{\partial x_2}{\partial x_3} \quad \frac{\partial \dot{x}_1}{\partial x_3} \quad \frac{\partial \dot{x}_2}{\partial x_3}\right]^T = \left[0 \quad 0 \quad \frac{L_q}{L_d} n_p x_2 \quad \frac{L_d}{L_q} n_p x_1 - \frac{1}{L_q} n_p \lambda_f\right]^T \tag{13}$$

The rank(A) = 1 is calculated according to (13). In order to estimate x_m, it is necessary to establish the left inverse system model of the speed subsystem. Therefore, the following form is established.

$$\boldsymbol{Z}_m = [\dot{x}_1] \tag{14}$$

After taking the partial derivative of the system in (14) with respect to the rotational speed component, its rank is

$$\det\left(\frac{\partial \boldsymbol{Z}_m}{\partial x_3}\right) = \frac{L_q}{L_d} n_p x_2 \neq 0 \tag{15}$$

The speed inner sensor model is therefore kept invertible. The left inverse system can be theoretically stated as follows.

$$\boldsymbol{x}_{um} = f(\boldsymbol{x}_m, \boldsymbol{Z}_m, \boldsymbol{u}) = f(i_d, i_q, \dot{i}_d, u_d, u_q) \tag{16}$$

3.3. Establishment of the Fuzzy Neural Network Left Inverse System

3.3.1. Control Principle of Fuzzy Neural Network

As two components of intelligent control field, fuzzy control and neural network have obvious advantages and disadvantages. For example, the former has excellent self-learning and adaptive ability, but due to the use of a black box, it cannot directly reveal the calculation process. The latter can select relevant fuzzy rules and membership functions according to their own requirements, but this method lacks adaptability. Fuzzy rules and membership functions are artificially set according to knowledge and experience, which is subjective. The fusion of the two is the only way for the development of intelligent control field, and fuzzy neural network came into being.

At present, scholars have proposed various types of fuzzy neural networks, and each type has its own characteristics. A adaptive neural fuzzy inference system (ANFIS) is used in this section. By implementing the Takagi-Sugeno (T-S) fuzzy reasoning model into practice, ANFIS is produced. Researchers have conducted extensive study and produced a number of discoveries because ANFIS can approximate nonlinear systems with arbitrary precision and is more practical and efficient than other kinds of fuzzy neural networks. The ANFIS structure with five inputs and one output is depicted in Figure 3. The ANFIS structure with five inputs and one output is depicted in Figure 3. Assume that

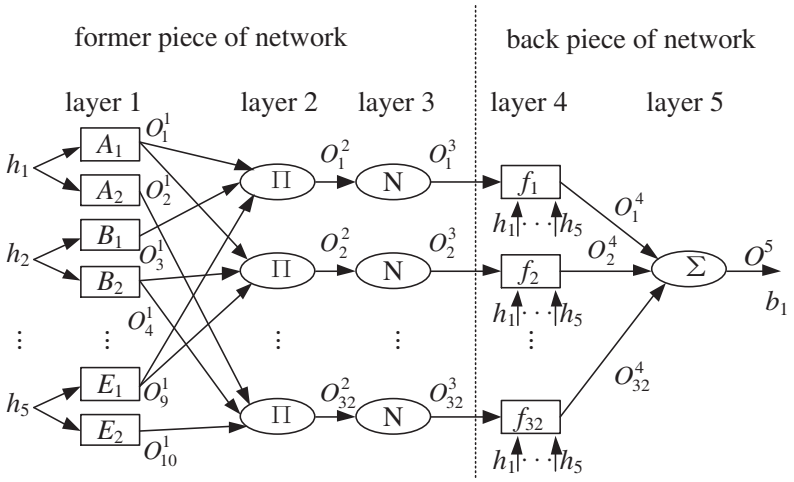

Figure 3. The ANFIS structure.

there are two membership functions — one for the front network and one for the back network — for each input. The fuzzy rule is generated by the back network, while the front network is utilized to match the fuzzy rule's antecedent. In Figure 3, $(h_1, h_2, h_3, h_4, h_5)$ are the inputs of ANFIS; b_1 is the output of ANFIS; and $(A_1, A_2, b_1, \ldots, E_2)$ are fuzzy sets. According to T-S fuzzy inference model, ANFIS IF-THEN fuzzy rule base can be written as

Rule 1: IF h_1 is A_1 and h_2 is B_1 and ... and h_5 is E_1, THEN $f_1 = P_{1,1}h_1 + P_{1,2}h_2 + \ldots + P_{1,5}h_5 + P_1$;

Rule 2: IF h_1 is A_2 and h_2 is B_1 and ... and h_5 is E_1, THEN $f_2 = P_{2,1}h_1 + P_{2,2}h_2 + \ldots + P_{2,5}h_5 + P_2$;

...

Rule 32: IF h_1 is A_2 and h_2 is B_2 and ... and h_5 is E_2, THEN $f_32 = P_{32,1}h_1 + P_{32,2}h_2 + \ldots + P_{32,5}h_5 + P_{32}$;

Layer 1: The membership function value of each input in the related fuzzy set is determined by this layer, which is a fuzzy layer. This layer has 10 nodes, and the output of each node can be expressed as

$$\begin{cases} O_1^1 = \mu_{A_1}(h_1) \\ O_2^1 = \mu_{A_2}(h_1) \\ O_3^1 = \mu_{B_1}(h_2) \\ \cdots \\ O_{10}^1 = \mu_{E_2}(h_5) \end{cases} \tag{17}$$

where $(\mu_{A_1}, \mu_{A_2}, \mu_{B_1}, \ldots, \mu_{E_2})$ is the membership function.

Gauss function is used as the membership function, and the specific form is

$$\mu(h) = e^{\frac{-(h-c)^2}{\sigma^2}} \tag{18}$$

where (c, σ) is the parameters of the former piece of network, which need to be identified in the training session.

Layer 2: Each node in this layer corresponds to a distinct fuzzy rule, and the AND algorithm is used to determine how adaptable the fuzzy rule is. The output of each of the 32 nodes, which there are in total, is as follows.

$$O_l^2 = \varepsilon_l = \mu_{A_{l1}}(h_1)\mu_{B_{l2}}(h_2)\mu_{C_{l3}}(h_3)\mu_{D_{l4}}(h_4)\mu_{E_{l5}}(h_5) \tag{19}$$

where l_1, l_2, l_3, l_4, $l_5 \in \{1, 2\}$, $l = 1, 2, \ldots, 32$.

Layer 3: This layer has the purpose of standardizing the fitness of the fuzzy rules produced in layer 2. There are 32 nodes in this layer, and the output of each node is as follows

$$O_l^3 = \bar{\varepsilon}_l = \varepsilon_l / \sum_{i=1}^{32} \varepsilon_i \tag{20}$$

Layer 4: The function of this layer is to find fuzzy rules and output fuzzy solutions according to corresponding rules. The number of nodes in this layer is also 32, and the output of each node is as follows

$$O_l^4 = \bar{\varepsilon}_l f_l = \bar{\varepsilon}_l (P_{l,1}h_1 + P_{l,2}h_2 + \ldots + P_{l,5}h_5 + R_l) \tag{21}$$

where $(P_{l,1}, P_{l,2}, P_{l,3}, P_{l,4}, P_{l,5})$ and R_l are the parameters of the back piece of network, and it also needs to be identified in the training session.

Layer 5: The computation algorithm for this layer, which is utilized to determine the ANFIS's ultimate output, is

$$O^5 = b_1 = \sum_{i=1}^{32} O_i^4 = \sum_{i=1}^{32} \bar{\varepsilon}_i f_i \tag{22}$$

3.3.2. Fuzzy Neural Network Left Inverse System

The PMSM is easily affected by the uncertainties of the changing parameters, so it is difficult to obtain the analytical left inverse system of the speed subsystem. To solve this problem, fuzzy neural

networks with excellent approximation ability are introduced into the left inverse system. The fuzzy neural network and differentiators are combined to construct the left inverse system of the PMSM speed subsystem. Because the PMSM is easily affected by the uncertainty of parameter changes, it is difficult to generate the analytical left inverse system of the speed subsystem. A fuzzy neural network with high approximation capabilities is added to the left inverse system to address this problem. The fuzzy neural network and differentiator are used to create the left inverse system of the PMSM speed subsystem. The nonlinear mapping relationship and the dynamic properties of the left inverse system are described by fuzzy neural network and differentiator, respectively. Formula (14) states that the differentiator is necessary for the left inverse system of the fuzzy neural network's speed subsystem. The derivatives of current, voltage, and current signals need to be taken as input samples, while the velocity signals need to be taken as output samples, so that ANFIS can be used to approximate the nonlinear mapping relationship of the left inverse system. In order to obtain the input and output samples required by ANFIS, a PMSM closed-loop control system is constructed. Adopt random signals within the working range and collect 3500 groups of data samples, of which 2500 groups are used for training, 500 groups used for verification, and the remaining 500 groups used for testing. The whole inputs are therefore i_d, i_q, i'_d, u_d, u_q and the output samples demanded by ANFIS ω_e.

The data from input and output are normalized to reduce sampling error and shorten training time. First, it is necessary to train ANFIS offline, set 4 membership functions for each input, and the former piece of network parameters (c, σ), back piece of network parameters $(P_{l,1}, P_{l,2}, P_{l,3}, P_{l,4}, P_{l,5})$ and R_l are adjusted by the sampling mixed algorithm, until the error of the ANFIS is less than the set value 0.001. The diagram of PMSM sensorless control structure based on the fuzzy neural network left inversion is shown in Figure 4.

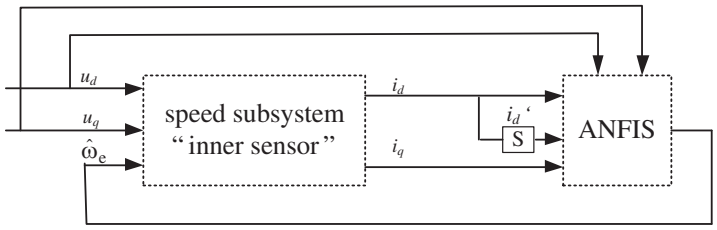

Figure 4. The diagram of PMSM sensorless control structure based on the fuzzy neural network left inversion.

3.3.3. Speed Sensorless Control Method for PMSM

Figure 5 depicts the overall block diagram of the control system. Using the proposed sensorless control method, taking d- and q-axis voltage and d- and q-axis current as inputs, the speed and rotor angle information are obtained through the sensorless control algorithm shown in Figure 5. Make the difference

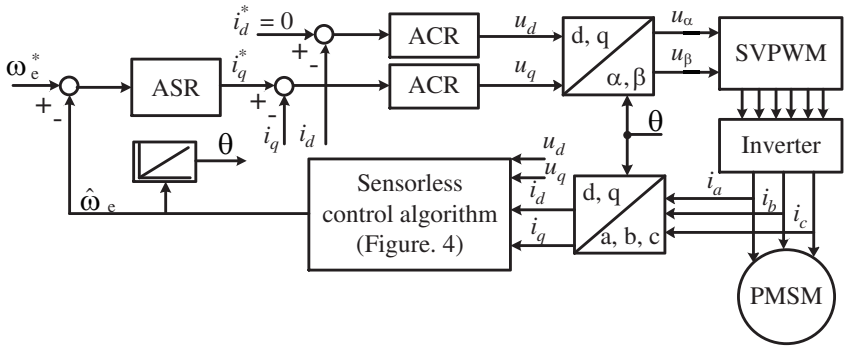

Figure 5. Total block diagram of PMSM sensorless control structure.

between the collected speed $\hat{\omega}_e$ and the given speed signal ω_e^*, and realize the speed closed-loop control through the proposed ADRC regulator in Section 2. After obtaining the current command signal i_d^* and i_q^*, make the difference with the collected current feedback signal i_d and i_q, and then realize the current closed-loop control through two current regulators ACR.

4. EXPERIMENTAL VERIFICATION

In order to verify the effectiveness of the proposed method, the speed, speed error, angle, and angle error in sensorless control of the PMSM are analyzed and verified experimentally. The test bench used in this experiment is shown in Figure 6. The main control board uses TI's TMS320F28335 DSP, the driver uses IPM modules, and integrates current sampling, bus voltage sampling, and optocoupler isolation circuits. The specific parameters of the motor are shown in Table 1. Using the model-based design method, the DSP programming process is completed in Matlab, and the data and running state of the motor are monitored by Matlab.

Table 1. Parameters of the prototype.

Parameters	Value	Parameters	Value
Stator resistance R (Ω) and inductance L_s (H)	1.6/0.005075	Rated power P (kW)	0.2
Pole Pairs	4	Rated voltage U (V)	220
Permanent magnet flux λ_f (Wb)	0.0825	Rated current I (A)	2.1
Rated speed n_N (r/min)	3000	Rated torque T_e (N·m)	0.64

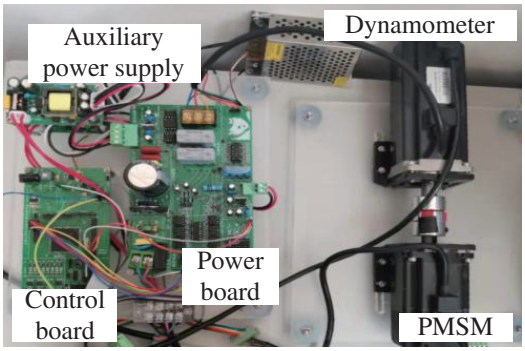

Figure 6. Schematic diagram of the experimental platform.

Figure 7 is the waveform of sensorless control at 30 r/min. The speed error waveforms with no load for the traditional control method based on the high-frequency injection and the proposed control method are both shown in Figure 7(a). As can be seen from Figure 7(a), the vibration amplitude of speed error with no load is 10 r/min and 8 r/min, respectively. The vibration amplitudes of the two are basically the same. Figure 7(b) shows the angle error waveforms with no load for the traditional control method and the proposed control method. The angle error vibration amplitude of the traditional method is 0.5 rad at no load, and that of the proposed method is 0.1 rad at no load. The angle error vibration amplitude of the proposed method is smaller than that of the traditional method. The angle tracking state in Figure 7(c) reflects the angle tracking effect of the traditional control method and the proposed method at no load. It can be seen from the figure that the effect of the proposed method is better than that of the traditional control method. The speed error waveforms with full load for the traditional control method based on the high-frequency injection and the proposed control method are both shown in Figure 7(d). As can be seen from Figure 7(d), the vibration amplitude of speed error

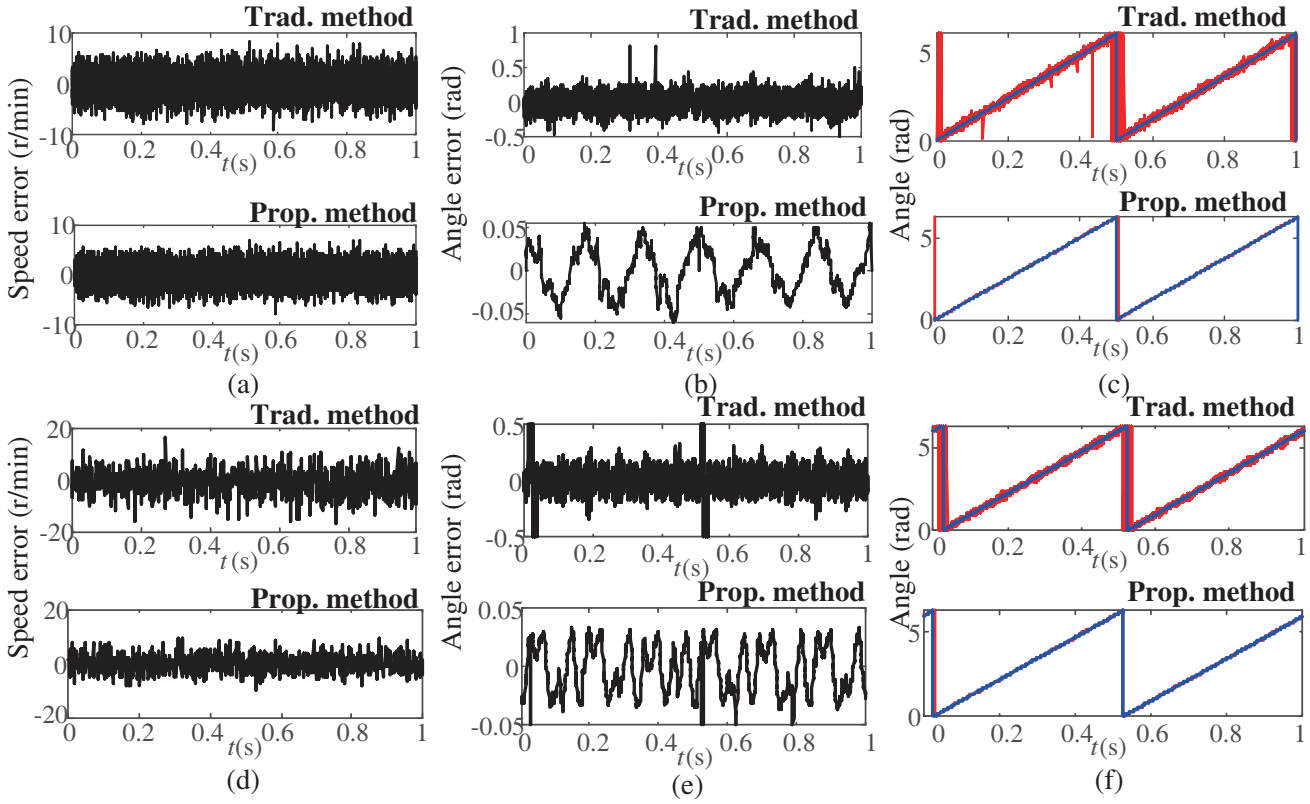

Figure 7. Speed error, angle value and angle error value at 30 r/min. (a) Speed error with no load. (b) Angle error with no load. (c) Angle value with no load. (d) Speed error with full load. (e) Angle error with full load. (f) Angle value with full load.

with full load is 36 r/min and 17 r/min, respectively. Figure 7(e) shows the angle error waveforms with full load for the traditional control method and the proposed control method. The angle error vibration amplitude of the traditional method is 1.0 rad at full load, and that of the proposed method is 0.08 rad at full load. The angle error vibration amplitude of the proposed method is smaller than that of the traditional method. The angle tracking state in Figure 7(f) reflects the angle tracking effect of the traditional control method and the proposed method at full load. It can be seen from the figure that the effect of the proposed method is better than that of the traditional control method.

Figure 8 is the waveform of sensorless control at 3000 r/min. The speed error waveforms with no load for the traditional control method based on the extended back EMF and the proposed control method are both shown in Figure 8(a). As can be seen from Figure Figure 8, the vibration amplitude of speed error with no load is 13 r/min and 8 r/min, respectively. Figure 8(b) shows the angle error waveforms with no load for the traditional control method and the proposed control method. The angle error vibration amplitude of the traditional method is 0.6 rad at no load, and that of the proposed method is 0.1 rad at no load. The angle error vibration amplitude of the proposed method is smaller than that of the traditional method. The angle tracking state in Figure 8(c) reflects the angle tracking effect of the traditional control method and the proposed method at no load. It can be seen from the figure that the effect of the proposed method is better than that of the traditional control method. The speed error waveforms with full load for the traditional control method and the proposed control method are both shown in Figure 8(d). As can be seen from Figure 8(d), the vibration amplitude of speed error with full load is 23 r/min and 15 r/min, respectively. Figure 8(e) shows the angle error waveforms with full load for the traditional control method and the proposed control method. The angle error vibration amplitude of the traditional method is 2.0 rad at full load, and that of the proposed method is 0.1 rad at full load. The angle error vibration amplitude of the proposed method is smaller than that of the

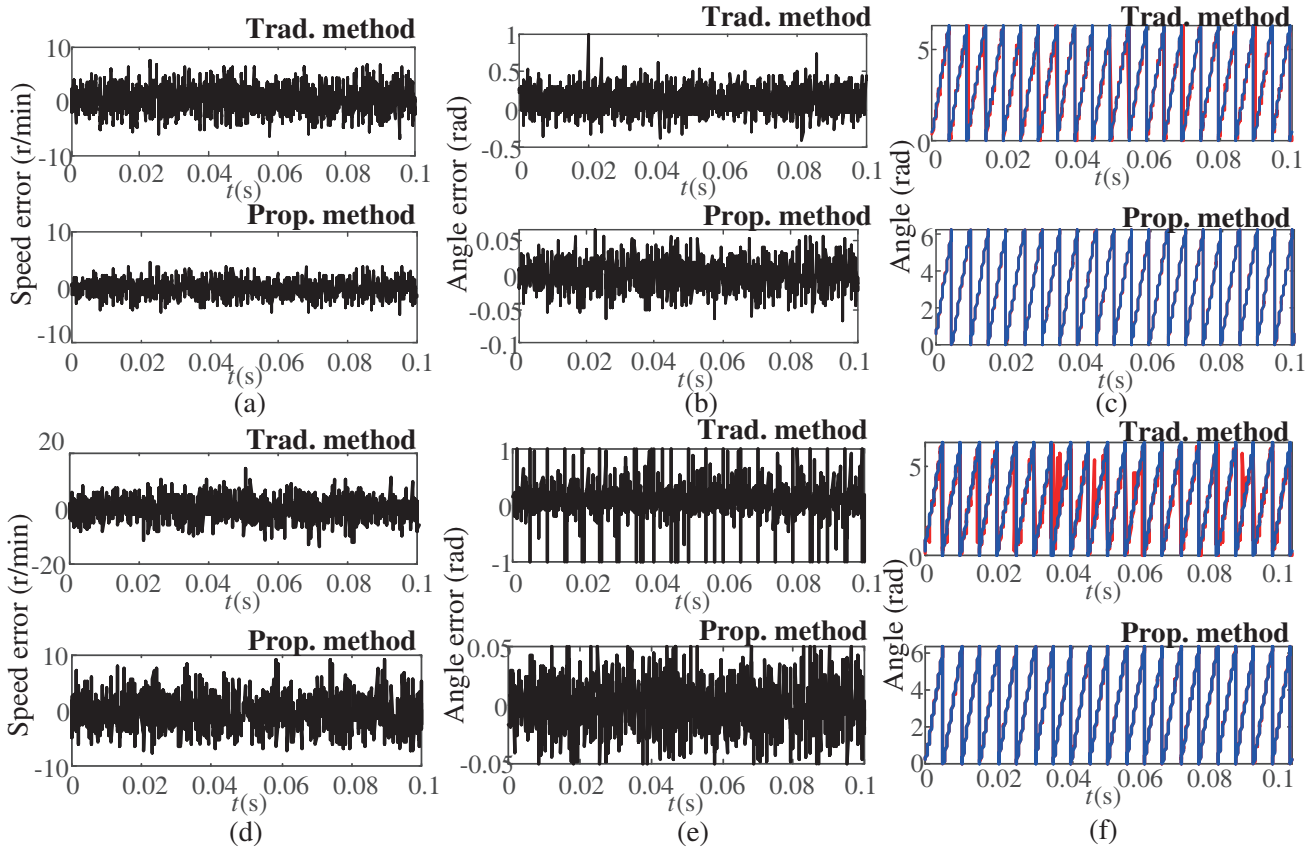

Figure 8. Speed error, Angle value and angle error value at 30 r/min. (a) Speed error with no load. (b) Angle error with no load. (c) Angle value with no load. (d) Speed error with full load. (e) Angle error with full load. (f) Angle value with full load.

traditional method. The angle tracking state in Figure 8(f) reflects the angle tracking effect of the traditional control method and the proposed method at full load. It can be seen from the figure that the effect of the proposed method is better than that of the traditional control method.

It can be seen from Table 2 that the proposed method has good control performance at both low speed and high speed. At the same time, the experimental data in [3] are also listed, and the data results are similar to those in this paper.

Table 2. Experimental data.

			Trad. Method	Prop. Method	Control method in [2]
low speed	no load	Speed error (r/min)	10	8	-
		Angle error (rad)	0.5	0.1	-
	full load	Speed error (r/min)	36	17	-
		Angle error (rad)	1	0.08	-
high speed	no load	Speed error (r/min)	13	8	10
		Angle error (rad)	0.6	0.1	0.34
	full load	Speed error (r/min)	23	15	-
		Angle error (rad)	2	0.1	-

5. CONCLUSIONS

A sensorless control method based on active disturbance rejection control (ADRC) and left inverse of fuzzy neural network for PMSM is proposed in this paper. The following is a summary of the major contributions: (1) After determining the left reversibility of the PMSM control system, the fuzzy neural network is utilized to build the left inverse system. The left inverse system is then coupled in series with the PMSM control system to realize the sensorless control of the PMSM. (2) The speed loop ADRC control is adjusted using the observed speed value, which enhances the effectiveness of the control system. (3) The proposed control approach is more general than both the extended back EMF method and the conventional high frequency injection method. Despite the good control impact of the suggested approach, the control algorithm has certain issues with computation and data storage. The development of an algorithm that requires less computing and data storage is required in later stages.

REFERENCES

1. Liu, X., Y. Pan and L. Wang, et al., "Model predictive control of permanent magnet synchronous motor based on parameter identification and dead time compensation," *Progress In Electromagnetics Research C*, Vol. 120, 253–263, 2022.
2. Pan, Y., X. Liu and Y. Zhu, et al., "A leading angle flux weakening control method for PMSM based on active disturbance rejection control," *Progress In Electromagnetics Research C*, Vol. 121, 2022.
3. Zhu, Y., Y. Bai, H. Wang, and L. Sun, "Sensorless control of permanent magnet synchronous motor based on t-s fuzzy inference algorithm fractional order sliding mode," *Progress In Electromagnetics Research M*, Vol. 105, 161–172, 2021.
4. Liang, G., S. Huang, and M. Li, "Mechanical parameter identification of permanent magnet synchronous motor based on high-order fast terminal sliding mode disturbance observer," *2019 22nd International Conference on Electrical Machines and Systems (ICEMS)*, 1–6, Harbin, China, 2019.
5. Woldegiorgis, A., X. Ge, S. Li, and M. Hassan, "Extended sliding mode disturbance observer-based sensorless control of IPMSM for medium and high-speed range considering railway application," *IEEE Access*, Vol. 7, 175302–175312, 2019.
6. Lin, Z., Q. Geng, Z. Zhou, X. Li, and C. Xia, "MTPA control of sensorless IPMSM based on high frequency square-wave signal injection," *2019 IEEE Applied Power Electronics Conference and Exposition (APEC)*, 2577–2581, Anaheim, USA, 2019.
7. Zhang, Y., Z. Yin, J. Liu, R. Zhang, and X. Sun, "IPMSM sensorless control using high-frequency voltage injection method with random switching frequency for audible noise improvement," *IEEE Transactions on Industrial Electronics*, Vol. 67, No. 6, 6019–6030, 2019.
8. Et-taaj, L., Z. Zakaria, A. El Kharki, et al., "Improvement of sensorless control of induction motor by voltage source inverter nonlinearities compensation and extended Kalman filter," *Electrical Engineering*, 1–13, 2022.
9. Pasqualotto, D., S. Rigon, and M. Zigliotto, "Sensorless speed control of synchronous reluctance motor drives based on extended kalman filter and neural magnetic model," *IEEE Transactions on Industrial Electronics*, Vol. 70, 1321–1330, 2023.
10. Liu, Z., J. Nie, H. Wei, et al., "Switched PI control based MRAS for sensorless control of PMSM drives using fuzzy-logic-controller," *IEEE Open Journal of Power Electronics*, Vol. 3, 368–381, 2022.
11. Huang, Y., J. Zhang and D. Chen, et al., "Model reference adaptive control of marine permanent magnet propulsion motor based on parameter identification," *Electronics*, Vol. 11, 1012, 2022.
12. Zhang, Z., "Sensorless control of synchronous machines using fundamental back-EMF voltage — A review," *IEEE Transactions on Power Electronics*, 2022.
13. Hua, Y. and H. Zhu, "Sensorless control of bearingless permanent magnet synchronous motor based on LS-SVM inverse system," *Electronics*, Vol. 10, No. 3, 265, 2021.